

3D Crowd Counting via Geometric Attention-guided Multi-View Fusion

Qi Zhang · Antoni B. Chan

Received: date / Accepted: date

Abstract Recently multi-view crowd counting using deep neural networks has been proposed to enable counting in large and wide scenes using multiple cameras. The current methods project the camera-view features to the average-height plane of the 3D world, and then fuse the projected multi-view features to predict a 2D scene-level density map on the ground (i.e., birds-eye view). Unlike the previous research, we consider the variable height of the people in the 3D world and propose to solve the multi-view crowd counting task through 3D feature fusion with 3D scene-level density maps, instead of the 2D density map on the ground-plane. Compared to 2D fusion, the 3D fusion extracts more information of the people along the z -dimension (height), which helps to address the scale variations across multiple views. The 3D density maps still preserve the 2D density maps property that the sum is the count, while also providing 3D information about the crowd density. Furthermore, instead of using the standard method of copying the features along the view ray in the 2D-to-3D projection, we propose an attention module based on a height estimation network, which forces each 2D pixels to be projected to one 3D voxel along the view ray. We also explore the projection consistency among the 3D prediction and the ground-truth in the 2D views to further enhance the counting performance. The proposed method is tested on the synthetic and real-world multi-view counting datasets and achieves better or comparable counting performance to the state-of-the-art.



Fig. 1 An example for the limitation of single-view counting for large and wide scenes: limited field-of-view, low resolution and severe occlusion. This image is from the ShanghaiTech dataset (Zhang et al. 2015).

1 Introduction

Single-view crowd counting has been studied extensively and has achieved promising performance on the existing counting datasets (Zhang et al. 2015; Idrees et al. 2013; Zhang and et al. 2016; Chan et al. 2008; Chen et al. 2012; Idrees and et al. 2018). However, in real-world applications, there are several situations where single-view counting cannot perform well (e.g., see Fig. 1): 1) the scene is too wide (such as a park or a football match stadium) where a single camera’s field-of-view is limited and cannot cover the whole scene; 2) the scene is too long (such as the underground train platform) where the people who are far away from the camera have very low resolution and the counting performance drops on these people; 3) the scene contains many obstacles, such as vehicles, building structures, *etc.*, where many people are heavily or totally occluded. Under the 3 conditions, the current single-view counting methods are inaccurate, because many people are miscounted

Qi Zhang
Shenzhen University, City University of Hong Kong
E-mail: qzhang364-c@my.cityu.edu.hk

Antoni B. Chan
City University of Hong Kong
E-mail: abchan@cityu.edu.hk

due to limited field-of-view, low resolution and severe occlusion.

To address the aforementioned situations, multiple cameras should be deployed, and the multi-view information should be fused to enhance the counting performance for complicated scenes. A few works (Li et al. 2012; Ryan et al. 2014; Tang et al. 2014; Ge and Collins 2010) have considered multi-view counting, but the hand-crafted features and the foreground extraction steps limit their performance. Recently, a CNN-based multi-view counting method (Zhang and Chan 2019) was proposed, which improved the counting performance on wide-area scenes through the use of view fusion with deep neural networks. Zhang and Chan (2019) projected the multi-view information (camera-view density maps or feature maps) to a 2D plane (at the height of a person) in the 3D scene, and then fused them to predict the 2D scene-level density maps on the ground-plane. Several fusion methods are considered, including late and early fusion, and a multi-view multi-scale early fusion model (MVMS), which handles both the inter- and intra-view scale variations.

The disadvantage of the 2D-to-2D projection used by Zhang and Chan (2019) is that the features of the same person from different views may not line up correctly due to the approximation that all features come from the same height in the 3D world. Clearly this is not true for features extracted from the head and feet of a person. To address this problem, in this paper, we propose to use 3D projection and 3D feature fusion to perform the multi-view counting task. Our proposed method consists of the following components (see Fig. 2): 1) *single view feature extraction and density map prediction*: 2D single-view features are extracted and then decoded to the 2D density map predictions; 2) *2D-to-3D projection*: a differentiable projection layer together with the camera parameters are used to perform the fixed 3D projection from image plane to 3D world; 3) *3D fusion and prediction*: the projected multi-view 3D features are fused using 3D CNN layers to predict the 3D scene-level density map ; 4) *Projection consistency between the 3D prediction and 2D views*: the 3D prediction is back-projected to each camera view and a loss between the camera view prediction and back-projected 3D prediction is added to enhance the multi-view counting performance.

In our approach, the 3D projection provides more information about each person along the z -dimension (height). We notice that the 2D-to-3D projection used in many DNNs-based multi-view fusion methods Zhang and Chan (2019); Kar et al. (2017); Isakov et al. (2019) form the 3D feature map by copying 2D features along the view-ray in the 3D volume. This violates the prin-

ciple that each 2D pixel should only come from one 3D voxel. To consider this geometric constraint between 3D and 2D space, we propose a geometric attention mechanism along the projection view ray by estimating the probable pixel height in the 3D world. In addition, a 3D density map with 3D Gaussian kernels is used to represent the crowd in the scene, instead of a 2D scene-level density map. The 3D density map can provide more information about the crowd in 3D, e.g., the elevation of the crowd.

In summary, the main contributions of our paper are as follows:

- We propose an end-to-end DNNs-based 3D multi-view counting method that predicts 3D density maps, which provides information about the crowd in 3D.
- Unlike previous methods, we use 3D projection and 3D fusion, which can help to deal with the scale variation issue without the scale selection module.
- We consider the geometry in the projection and propose an attention module along the view ray for better 2D-to-3D projection.
- The projection consistency between the camera-view ground-truth and the back-projected 3D predictions is explored to further boost the multi-view counting performance. The proposed method can achieve better or comparable counting performance to the state-of-art.

The remainder of this paper is organized as follows. In Section 2, we review the existing single-view and multi-view counting methods, as well as 3D object reconstruction using deep neural networks (DNNs). In Section 3, we introduce the proposed 3D multi-view counting method including the 3D fusion and geometric attention module. In Section 4, we show the experiments settings and results, and conclude in Section 5.

2 Related Work

In this section, we review the existing single-view and multi-view counting methods. We also review 3D object reconstruction using deep neural networks (DNNs). A preliminary conference version of this paper appears in AAAI (Zhang and Chan 2020). This journal paper extends the conference version in terms of following aspects: 1) a geometric-guided attention module along the view ray is proposed to reduce the feature redundancy caused by the previous 2D-to-3D projection steps; 2) updated 3D counting performance on the DukeMTMC dataset, which is better than in the previous conference version; 3) More experiments on more multi-view counting datasets to better validate the proposed method.

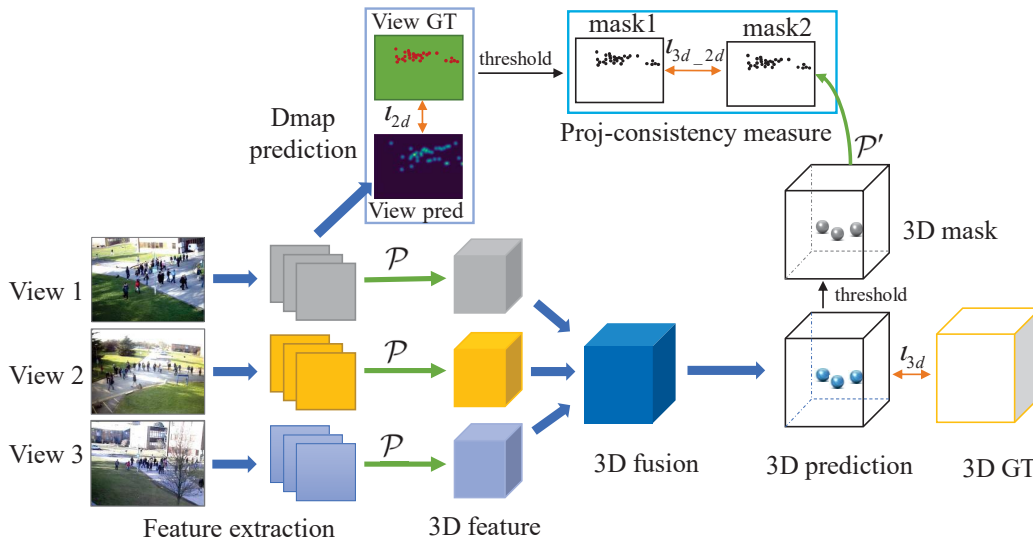


Fig. 2 The pipeline of 3D crowd counting. Single-view features are extracted and then projected to the 3D world on multiple height planes. The projected 3D features are concatenated and fused to output the 3D density map prediction (loss l_{3d}). Each camera-view prediction branch decodes the 2D features to obtain the 2D camera-view predictions (loss l_{2d}). Finally, the 3D prediction is back-projected to each camera-view, and the the projection consistency between the camera-view ground-truth and the back-projected prediction is measured (loss l_{3d-2d}).

2.1 Single-view counting

Single-view crowd counting has achieved satisfactory performance on the existing counting datasets, especially the DNN-based density map estimation methods (Sindagi et al. 2020; Jiang et al. 2020; Bai et al. 2020; Yang et al. 2020). Zhang et al. (2015) proposed a single-column CNN framework to directly estimate the density maps from the images. Scale variations due to perspective changes is a critical issue in the crowd counting task, which can limit the performance, and many methods have been proposed to handle scale variations (Boominathan et al. 2016; Zhang and et al. 2016; Sam et al. 2017; Kang and Chan 2018; Onoro-Rubio and López-Sastre 2016). Sindagi and Patel (2017) proposed the contextual pyramid CNN (CP-CNN) to incorporate global and local context information in the crowd counting framework. Furthermore, extra information and more sophisticated networks were utilized to further improve the counting performance (Idrees and et al. 2018; Wang et al. 2019; Ranjan et al. 2018; Cao et al. 2018; Li et al. 2018; Liu et al. 2018; Shen et al. 2018; Jiang and et al. 2019; Liu et al. 2019). Kang et al. (2017) proposed an adaptive convolution neural network (ACNN) by utilizing the context (camera height and angle) as side information in the counting framework. Shi et al. (2019) integrated the perspective information to provide additional knowledge of the person scale change in an image. Lian et al. (2019) proposed a regression guided detection network (RDNet) for RGB-D crowd counting. Liu and et al. (2019) pro-

posed Recurrent Attentive Zooming Network to zoom high density regions for higher-precision counting and localization. Besides methods relying on density map for supervision, methods utilizing other forms of supervision are also proposed, such as classification (Xiong et al. 2019), local counting map (Liu et al. 2020), and dot maps (Wang et al. 2020; Ma et al. 2019).

The single-view based counting methods cannot handle the situations when the camera view cannot capture the whole scene, the occlusions in the scene are too severe, or the people are in low resolution due to long distance from the camera. Therefore, multiple cameras should be adopted to improve the counting performance for these wide-area scenes.

2.2 Multi-view counting

Traditional multi-view counting methods can be divided into 3 categories: detection/tracking based (Dittrich et al. 2017; Li et al. 2012; Ma et al. 2012; Maddalena et al. 2014), regression based (Ryan et al. 2014; Tang et al. 2014), and 3D cylinder based methods (Ge and Collins 2010). These multi-view counting methods have several limitations. First, they need to utilize foreground extraction techniques to segment the crowd from background. Therefore, the effectiveness of the foreground extraction step limits the final counting performance. Second, hand-crafted features are used both in the people detection or crowd count regression. The hand-crafted features lack representation ability, which reduces the

robustness and the performance of the methods. Third, these methods are mainly developed and tested on the PETS2009 (Ferryman and Shahrokni 2009), which is a multi-view dataset with small crowd numbers and staged crowd behavior.

Recently, Zhang and Chan (2019) proposed a DNN-based multi-view counting method and a new larger multi-view counting dataset, CityStreet. This multi-view multi-scale (MVMS) DNN first extracts camera-view information (density maps or features), and then projects them to the average-height plane in the 3D scene with the given camera parameters. Next, the projected features are fused and decoded to predict the scene-level density maps (on the average height plane). Our proposed method differs from MVMS in the several aspects: 1) instead of using average-height projection (2D-2D projection), we use multi-height projection (2D-3D projection), which spatially aligns the person’s features (e.g., head, body and feet features) in 3D, making it easier to find the geometric correspondence across views (See Fig. 4); 2) we predict a 3D crowd density map, generated using 3D Gaussian kernels, which provides distribution of the crowd in 3D space; 3) the 3D density map prediction is back-projected to each camera view, and compared with the 2D ground-truth density map of the camera view, which defines a projection consistency loss for improving the accuracy.

2.3 DNN-based 3D reconstruction

Our 3D crowd counting method is related to a few works on DNN-based 3D object reconstruction and human pose estimation. Yan et al. (2016) proposed an unsupervised single-view 3D object reconstruction method utilizing the projection loss defined by the perspective transformation. Choy et al. (2016) proposed a 3D RNNs architecture to gradually refine the multi-view 3D object reconstruction step-by-step. Kar et al. (2017) leveraged the 3D geometry constraint of features through projection and unprojection operations in the 3D reconstruction method. Huang et al. (2018) presented DeepMVS to produce a set of plane-sweep volumes and then predict high-quality disparity maps. Isakov et al. (2019) proposed two learnable triangulation methods for 3D human pose estimation: algebraic triangulation and volumetric aggregation.

It can be observed that the existing DNNs-based 3D reconstruction methods are mainly focused on the reconstruction of a single object (e.g., see the ShapeNet (Chang and et al. 2015) and IKEA (Lim et al. 2013) datasets, or human pose). Our proposed method can also be regarded as predicting a 3D representation from

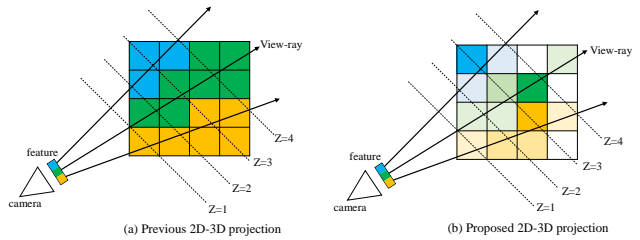


Fig. 3 The 2D-3D projection process. (a) previous projection forms the 3D grids by copying the 2D features along the view-ray to the 3D grids with intersection; and (b) the proposed geometric attention guided 2D-3D projection process, which forces one 2D feature to be projected to one 3D voxel and other grids are suppressed. On the right, lighter colors indicates lower probability of the 3D voxel coming from the corresponding 2D feature along the view-ray.

multiple viewpoints, but differs from the existing DNN-based 3D object reconstruction in several aspects. First, the proposed method can do more than 3D shape reconstruction, because the 3D Gaussian kernels can represent the crowd’s 3D distribution as well as indicate the crowd count. Second, unlike the previous 3D object reconstruction, the proposed method targets at the scene-level representation (all people in the scene), not only a single object. Furthermore, we exploit the relationship between the 2D camera-view density maps and 3D scene-level density maps to obtain a projection consistency loss.

2.4 2D-to-3D projection in CNNs

For DNNs-based multi-camera fusion tasks, such as 3D reconstruction from multi-view images (Kar et al. 2017) or 3D human pose estimation (Isakov et al. 2019), the projection modules are used to project multi-view 2D features to the same 3D space for fusion (see Fig. 3a). According to the ideal camera pin-hole calibration model, a 2D image coordinate corresponds to multiple 3D locations along the view ray, since the Z -dimension coordinate is unknown. To handle this ill-posed problem, several approximation methods are utilized to form the 2D-to-3D projection operation in DNNs.

Kar et al. (2017) proposed the differentiable unprojection operation to project the 2D single-view image features into 3D space via copying the 2D features to the 3D voxels along the view ray. Many 3D reconstruction and 3D pose estimation methods have adopted this projection operation for multi-view fusion. However, the 3D voxels along the same view ray share the same features, which introduces redundancy in the 3D feature representation. Sitzmann et al. (2019) added an occlusion reasoning module for handling occlusion in the 3D-to-2D projection. Zhang and Chan (2019) were

Single-view branch		3D Fusion module	
Layer	Filter	Layer	Filter
Feature extraction		concatenation	-
conv 1	$16 \times 1 \times 5 \times 5$	3D conv 1	$32 \times n \times 5 \times 5 \times 7$
conv 2	$16 \times 16 \times 5 \times 5$	3D conv 2	$64 \times 32 \times 5 \times 5 \times 7$
pooling	2×2	3D conv 3	$128 \times 64 \times 5 \times 5 \times 7$
conv 3	$32 \times 16 \times 5 \times 5$	3D conv 4	$64 \times 128 \times 5 \times 5 \times 7$
conv 4	$32 \times 32 \times 5 \times 5$	3D conv 5	$32 \times 64 \times 5 \times 5 \times 7$
pooling	2×2	3D conv 6	$32 \times 32 \times 5 \times 5 \times 7$
Density map prediction		3D conv 7	$1 \times 32 \times 5 \times 5 \times 7$
conv 5	$64 \times 32 \times 5 \times 5$		
conv 6	$32 \times 64 \times 5 \times 5$		
conv 7	$1 \times 32 \times 5 \times 5$		

Table 1 The layer settings for the camera-view feature extraction and density map prediction branches (left), and the 3D fusion module (right). The filter dimensions are output channels, input channels, and filter size $w_0 \times h_0 \times d_0$ ($d_0 = 1$ in 2D conv layers).

the first to utilize DNNs for multi-view crowd counting. In their work, the multi-view features were projected to the average-height plane in the 3D space for fusion, which means each pixel’s height (Z -dimension in their calibration model) is assumed to be average height of a person (1.75m). In the conference version of this paper (Zhang and Chan 2020), the 2D features are projected to multiple heights to handle the wrong projection for other people body parts as in (Zhang and Chan 2019). However, the feature redundancy caused by the feature copying still exists, which results in fusion ambiguity across camera views. To alleviate the problem of feature redundancy in the projection step, we propose an attention module along the view ray to reduce the influence of repeated features in the 3D feature map on the multi-view fusion and decoding nets.

3 3D Counting via 3D Projection and Fusion

We follow the setup of multi-view counting from Zhang and Chan (2019): we assume fixed cameras with known intrinsic and extrinsic camera parameters, and synchronized camera frames across views. In contrast to Zhang and Chan (2019), which is based on 2D ground-plane density maps, we generate 3D ground-truth density maps by convolving the 3D ground-truth annotations with fixed-width 3D Gaussian kernels. The 3D ground-truth annotation coordinates are calculated from the 2D view annotations and people correspondence across views (see Section 4 for more details).

In this section, we introduce the end-to-end DNN-based 3D crowd counting method consisting of the following stages: 1) *Single view feature extraction and density map prediction*: 2D single-view features are extracted and decoded to predict a 2D camera-view density map; 2) *2D-to-3D projection*: a differentiable projection layer using the camera parameters projects the camera-view feature maps from the image plane to mul-

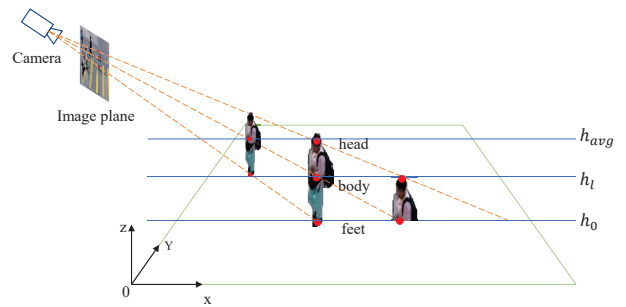


Fig. 4 The multi-height projection can extract feature of a person along the z dimension and form a 3D feature representation for the person, which is consistent with the 3D scene.

multiple height-planes in the 3D world; 3) *3D fusion and prediction*: the projected multi-view 3D features are fused to predict the 3D density maps using 3D CNN layers; 4) *Projection consistency between the 3D prediction and 2D views*: the 3D prediction is back-projected to each camera view, and then compared with the corresponding camera-view 2D ground-truth using loss to refine the 3D prediction.

3.1 Single-view branch

Each camera-view image is fed into a CNN to extract the camera-view features. The 2D camera-view features are decoded by another CNN to predict the camera-view density maps. The camera-view feature extraction and density map prediction layer settings can be found in Table 1 left.

The camera-view prediction branches contribute to the model performance in two aspects. First, the camera-view prediction branches together with the 2D density map supervision improve the training of the camera-view feature extraction. A similar strategy is used by Zhang and Chan (2019), where the camera-view prediction branches are used in the first stage for pre-training. Second, the camera-view prediction branches force the 2D feature representation to be consistent with the 3D feature representation, and the difference between them is the geometric projection. This constraint is natural because the 2D and 3D observations are linked by the geometric projection, and the same link still exists between the 2D and 3D feature representations. The 2D-3D feature representation constraint was also used by Girdhar et al. (2016) for 3D reconstruction, where the 3D representation is forced to be able to predict the corresponding 2D observations. Furthermore, this constraint can improve the final 3D prediction performance (see ablation study for more details).

Suppose there are N camera-views, the density map prediction for the i_{th} view is $V_i \in R^{h \times w}$ and the corre-

sponding ground-truth is $V_i^t \in R^{h \times w}$, then the camera-view density map prediction loss l_{2d} is the mean-square error (MSE):

$$l_{2d} = \frac{1}{wh} \sum_{i=1}^N \|V_i - V_i^t\|_2^2. \quad (1)$$

3.2 2D-to-3D projection

The extracted camera-view features are projected to the 3D world with a fixed 2D-to-3D projection layer. We assume that the camera intrinsic and extrinsic parameters are both known, which are used to perform the projection. Since each image pixel’s corresponding height in the 3D world is unknown, a height range H is used in the projection, where each pixel is projected to the 3D world multiple times onto different height planes. Then, the projected features from all heights are concatenated along the z -dimension to form a 3D feature representation. The 2D-to-3D projection layer can be implemented using the Sampler from the Spatial Transformer Networks (Jaderberg et al. 2015) with the known camera calibration parameters (intrinsic and extrinsic). Suppose that \mathcal{P} is the 2D-to-3D projection, F_i is the 2D feature presentation of view i , and the height range $H = \{h_0, h_1, \dots, h_r\}$, then the projected 3D feature representation $(F_{3d})_i$ for view i is

$$(F_{3d})_i = \mathcal{P}_i(F_i, H) = [\mathcal{P}_i(F_i, h_0), \dots, \mathcal{P}_i(F_i, h_r)], \quad (2)$$

where $[\cdot]$ is concatenation along the z -dimension (height).

The previous work of Zhang and Chan (2019) used the fixed-height projection, where all pixels were projected to the average person height (1750mm). Compared to the average-height projection, the multi-height projection can output a body feature representation along the z -dim (e.g., head, body and feet features, see Fig. 4), which allows the network to better identify the location of the person through the 3D alignment of the features.

3.3 Geometric attention along the view ray

To enforce the geometric constraint that a 2D pixel should be projected to only one 3D voxel, we propose an attention module along the view ray. The attention module reduces the feature redundancy caused by copying the same 2D feature along the view ray in the typical 2D-to-3D projection step. The main idea is to project different body parts of the people to different height levels, which is different from projecting all to the same

Attention along the view-ray	
Layer	Filter
Feature extraction	
conv 1	$64 \times 1 \times 3 \times 3$
conv 2	$64 \times 64 \times 3 \times 3$
pooling	2×2
conv 3	$128 \times 64 \times 3 \times 3$
conv 4	$128 \times 128 \times 3 \times 3$
pooling	2×2
conv 5	$256 \times 128 \times 3 \times 3$
conv 6	$256 \times 256 \times 3 \times 3$
conv 7	$256 \times 256 \times 3 \times 3$
Height map estimation	
conv 8	$128 \times 256 \times 5 \times 5$
conv 9	$64 \times 128 \times 5 \times 5$
conv 10	$N \times 64 \times 5 \times 5$
softmax layer	-
resize layer	if applicable

Table 2 The layer settings for the geometric attention module, including the feature extraction part and the height map estimation part. N stands for the height level number in the height maps, which is 7 for PETS2009 and CityStreet, or 5 for DukeMTMC. For CityStreet, an extra resize layer is used to resize the height maps’ z -dim to be 28; For DukeMTMC, zero padding along the z -dim is first adopted to increase height maps’ z -dim size to be 9 and then resized to 36.

height level as in (Zhang and Chan 2019), and projecting to all height levels like in 3D reconstruction.

A height prior can be incorporated in the model that the bottom body part is lower than the top part in the 3D world. Therefore, by dividing the human bounding boxes into several regions vertically, each region is assigned to a different height level. Note that the ground-truth bounding boxes are estimated from the people position annotations and camera calibrations (Zhang and Chan 2019), which does not need laborious annotation. As shown in Figure 5, we divide each bounding box into N parts, corresponding to N height levels. Thus, a $a \times b \times N$ binary map, denoted as height maps \mathcal{H} , is constructed as supervisory information, where the element \mathcal{H}_{ijh} indicates that the corresponding pixel (i, j) inside a bounding box belongs to the corresponding height level h . For background pixels (not within any bounding box), the corresponding height map entires are set to 0.

The geometric attention works as follows. First each 2D image pixel is classified into N height levels by a height map estimation CNNs (see the layer setting in Table 2). Then, the 2D map of each height class is projected to a 3D scene plane at its corresponding height level. In this way, the geometric constraint is enforced along the view ray. Finally, the 3D height map serves as the attention by multiplying with the 3D crowd counting feature map.

Suppose the height map prediction is $\mathcal{H} \in R^{a \times b \times N}$ and the corresponding ground-truth is $\mathcal{H}^t \in R^{a \times b \times N}$,

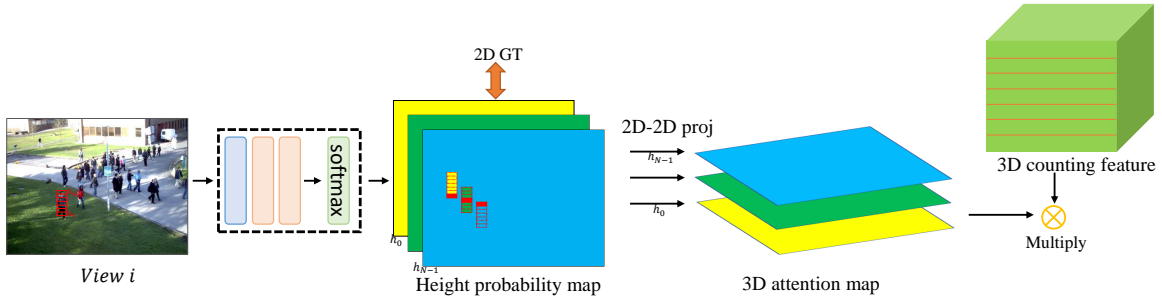


Fig. 5 The geometric attention module. Each pixel in the camera view image is classified into N height maps. The N height probability maps are projected to 3D scene planes according to their height levels (a set of 2D-2D projections for different height levels). The projected height maps are used as attention to reduce the repeated the features in the 3D counting feature via multiplication.

the height map prediction loss l_{hmap} is the MSE

$$l_{hmap} = \frac{1}{abN} \|\mathcal{H} - \mathcal{H}^t\|_2^2. \quad (3)$$

3.4 3D density map prediction

After the 2D-to-3D projection, the projected 3D features from multiple views are concatenated (along the feature channel) and then decoded by several 3D convolution layers. The architecture for the 3D feature decoder layers can be found in the right of Table 1. Let the 3D prediction be $G \in R^{a \times b \times N}$ and the corresponding ground-truth be $G^t \in R^{a \times b \times N}$. Then, the 3D prediction loss l_{3d} is the MSE

$$l_{3d} = \frac{1}{abN} \|G - G^t\|_2^2. \quad (4)$$

3.5 3D-to-2D projection consistency measure

Considering the geometric constraint between 2D camera plane and the 3D world, we also require the 3D prediction be consistent with the 2D single view density maps in terms of projection geometry. To achieve this, the 3D prediction G is projected to each camera-view i with a 3D-to-2D projection operation \mathcal{P}' . The projection consistency between the projected 2D density maps and the 2D density map ground-truth is measured and used as part of the loss to further enhance the 3D counting performance.

3D-to-2D projection. Let \mathcal{P}' be the 3D-to-2D projection, and \hat{G} be a 3D binary mask, which is the 3D prediction G thresholded at $T = 10^{-4}$. When performing the projection, without the height information, each 2D image point corresponds to many 3D points along the view ray. Therefore, the height range $H = \{h_0, h_1, \dots, h_r\}$ is also used in the 3D-to-2D projection. Then the projected 2D mask \hat{G}_i^{2D} for view i can be

denoted as,

$$\hat{G}_i^{2D} = \text{sign}\left(\sum_{l=0}^r \mathcal{P}'_l(\hat{G}, h_l)\right), \quad (5)$$

where \sum is summation along the z -dimension (height dimension). In the 3D-to-2D projection, the projected 2D pixel value can be regarded as the binary summation along the view ray in the 3D prediction grid (see Fig. 6).

Projection consistency measure. The main challenge to measure the consistency between the 3D density map prediction and the 2D camera-view density map is that some people who are occluded in a 2D camera-view will be present in the 3D prediction because they are visible from other views. Thus the MSE loss cannot be used directly here. Instead, we measure the consistency between the binary masks produced by thresholding the 3D prediction and the corresponding 2D ground-truth density map, while accounting for inconsistencies due to occlusions (see Fig. 6).

We define the 3D-to-2D projection consistency measure (PCM) for view i as

$$PCM_i = \frac{\|\hat{V}_i^t \otimes \hat{G}_i^{2D}\|_1}{\|\hat{V}_i^t\|_1 + \alpha}, \quad (6)$$

where \otimes denotes element-wise multiplication, \hat{V}_i^t is a binary mask computed by thresholding the ground-truth 2D density map of view i at 10^{-3} , \hat{G}_i^{2D} is the back-projected 3D prediction mask (see Eq. 5), and $\alpha = 10^{-5}$ is a constant to prevent divide-by-zero. The important property of the PCM is that no penalty occurs when an extra person is present in the 3D prediction \hat{G}_i^{2D} , but not the 2D camera-view (e.g., due to occlusion). On the other hand, the PCM will be reduced when a person in the 2D camera-view is missing in the 3D prediction. Finally, the projection consistency loss is defined by

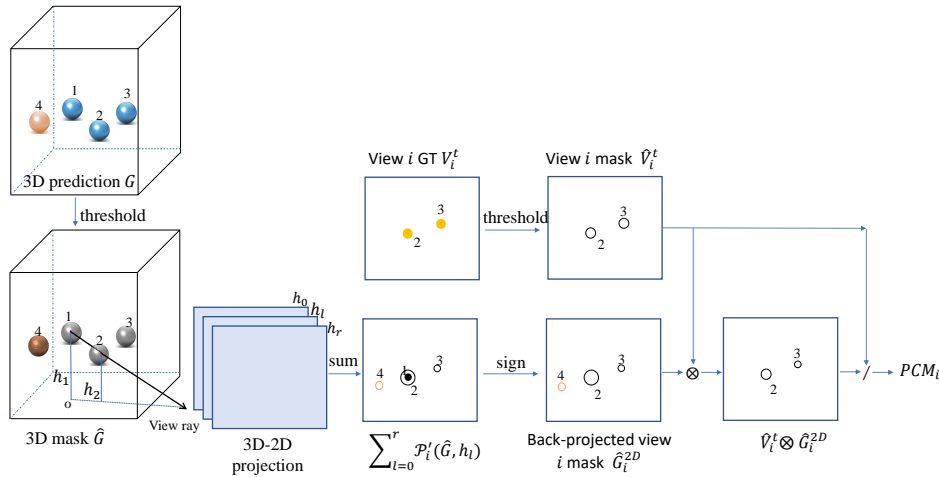


Fig. 6 Example of projection consistency measure (PCM). There are 4 people in the 3D prediction, while only Person 2 and Person 3 are visible in the 2D view i . Since Person 1 is occluded by Person 2 and Person 4 is totally occluded in view i , they are masked out in the PCM calculation. When the people location in the 3D prediction is not consistent with the 2D ground-truth, the PCM value is low.

summing over the camera-views:

$$l_{3d.2d} = \sum_{i=1}^N (1 - PCM_i). \quad (7)$$

3.6 Training loss

Combining all the aforementioned losses, the final loss is

$$l_{all} = l_{3d} + \beta l_{2d} + \gamma l_{3d.2d} + \sigma l_{hmap}, \quad (8)$$

where β , γ and σ are hyperparameters for weighting the contributions of each term.

4 Experiments and Evaluation

In this section, we will discuss the implementation details of the proposed 3D counting model, and conduct experiments on four multi-view counting datasets.

4.1 Implementation details

3D ground-truth generation. The 3D ground-truth is generated with the single-view annotations (here we use head annotations) and the cross-view correspondence, which are already available in the multi-view counting datasets. Suppose the same person’s corresponding annotations in M views ($M \leq N$) are $\{(x_j, y_j)\}$, $j \in \{1, 2, \dots, M\}$, their corresponding 3D coordinates are denoted as $\{W_j\} = \{\mathcal{P}_j((x_j, y_j, h))\}$ where the height

h is not known. Considering the projection correspondence, the 3D coordinate of the person’s head $W = [X, Y, Z]^T$ can be obtained by finding the height h that minimizes the spread of the projected head positions from all views,

$$Z = \operatorname{argmin}_h \|W_j - \bar{W}\|_2^2, \quad (9)$$

$$(X, Y) = \frac{1}{M} \sum_{j=1}^M \mathcal{P}_j((x_j, y_j, Z)), \quad (10)$$

where \bar{W} is the mean of $\{W_j\}$. Z is the height h minimizing (9), which can be obtained through searching h in the height range $H' \in \{h'_0, h'_1, \dots, h'_r\}$. In our experiments we use range $\{1000, 1010, 1020, \dots, 2000mm\}$. For numerical stability during training, 2D density ground-truth maps are scaled by 10^3 , while the 3D ground-truth is scaled by 10^4 . The predictions are scaled downward correspondingly for evaluation.

Training settings and methods. In the proposed method (see Fig. 2), besides the 3D counting prediction, there are two important modules: single-view density map prediction and the projection consistency measure module. In the ablation study, we show the influence of these two modules on the final 3D counting performance. A 3-stage training is used for the proposed method. In the first stage, $\beta = 1$ means that the single-view 2D supervision is dominant to benefit the feature extraction training. In the second stage, $\beta = 0.01$ means the 3D supervision is dominant to accelerate the 3D fusion training. In the third stage, $\beta = 0.01$ and γ is variable according to ground-truth setting, which increases the influence of the projection consistency measure (PCM) to further enhance the performance. In all

Dataset	PETS2009	DukeMTMC	CityStreet
Dmap weighted	8.32	2.12	9.36
Detection+ReID	9.41	2.20	27.60
Late fusion (Zhang and Chan 2019)	3.92	1.27	8.12
Naïve early fusion (Zhang and Chan 2019)	5.43	1.25	8.10
MVMS (Zhang and Chan 2019)	3.49	1.03	8.01
3D counting (ours)	3.15	1.01	7.54
3D counting+Attention (ours)	3.20	0.92	7.12

Table 3 Experiment results: mean absolute error (MAE) on three multi-view counting datasets. “3D counting” uses both single-view branches and the projection consistency measure loss. “3D counting+Attention” adds the geometric attention module to the 3D counting model.

stages, the learning rate is set as 10^{-4} and the batch size is 1.

4.2 Experiment setup

4.2.1 Datasets.

The proposed method is evaluated and compared on the 4 multi-view counting datasets, PETS2009 (Ferryman and Shahroki 2009), DukeMTMC (Ristani et al. 2016), CityStreet (Zhang and Chan 2019), and CVCS (Zhang and Chan 2021). We directly use the same dataset settings by Zhang and Chan (2019).

PETS2009 (Ferryman and Shahroki 2009) contains 3 views, and 1105 and 794 images are for training and testing, respectively. The input image resolution ($w \times h \times d$) is 384×288 and the 3D ground-truth resolution is $152 \times 177 \times 7$. The voxel height in z -dim is 40cm in the real world and the height range is 0 to 2.8m.

DukeMTMC (Ristani et al. 2016) contains 4 views, and the first 700 images are used for training and remaining 289 images are for testing. The input image resolution is 640×360 and the 3D ground-truth resolution is $160 \times 120 \times 36$. The voxel height in z -dim is 10cm in the real world and the height range is 0 to 3.6m. The larger height range is due to change of the ground height in the scene.

CityStreet (Zhang and Chan 2019) consists of 3 views and 500 images in which the first 300 are for training and remaining 200 for testing. The input image resolution is 676×380 and the 3D ground-truth resolution is $160 \times 192 \times 28$. The voxel height in z -dim is 10cm in the real world and the height range is 0 to 2.8m.

CVCS (Zhang and Chan 2021) is a large synthetic multi-view crowd counting dataset containing 31 scenes with around 100 camera views in each scene, where 23 scenes for training and 8 scenes for testing. The input image resolution is 640×360 . The 3D ground-truth resolution is $640 \times 720 \times 7$, and patch-based training is used and the cropped ground-truth size is $80 \times 90 \times 7$. The

	$n * h$	3D	3D+2D	3D+2D+PCM
PETS2009	7*40cm	4.12	3.20	3.15 ($\gamma = 100$)
	14*20cm	4.88	4.57	4.24 ($\gamma = 10$)
	28*10cm	5.34	4.27	4.21 ($\gamma = 1$)
DukeMTMC	9*40cm	1.82	1.71	1.65 ($\gamma = 10$)
	18*20cm	2.12	1.63	1.49 ($\gamma = 3$)
	36*10cm	2.15	1.03	1.01 ($\gamma = 0.1$)
CityStreet	7*40cm	8.98	8.49	8.35 ($\gamma = 100$)
	14*20cm	8.72	7.89	7.71 ($\gamma = 30$)
	28*10cm	7.87	7.58	7.54 ($\gamma = 10$)

Table 4 Ablation study of the training loss and ground-truth settings. γ is the hyperparameter for the projection consistency measure (PCM) loss. n is the number of voxels in the z -dimension (height), and h is the voxel height in the 3D world. The evaluation metric is MAE.

voxel height in z -dim is 40cm in the real world and the height range is 0 to 2.8m.

4.2.2 Comparison methods.

Five multi-view counting methods are used for comparison. 1) “Dmap weighted” fuses single-view density maps into a scene-level count with a view-specific weight map, which is constructed based on how many views can see a particular pixel. In the experiment, CSR-net (Li et al. 2018) is used to predict the single-view density maps for datasets PETS2009 and CityStreet, and FCN-7 for DukeMTMC. 2) “Detection + ReID” first detects all humans in each camera-view and then the scene geometry constraints and person ReID are used to associate the same people across views. Specifically, Faster-RCNN (Ren et al. 2015) is used for people detection and LOMO 2015 (Liao et al. 2015) for person ReID. 3) “late fusion” model fuses single-view density maps to predict 2D height-plane density maps (Zhang and Chan 2019); 4) “naïve early fusion” model fuses feature maps to predict 2D height-plane density maps (Zhang and Chan 2019); 5) “multi-view multi-scale (MVMS)” model fuses feature maps with a scale selection module to cope with the scale variation issue (Zhang and Chan 2019).

Evaluation metric. The mean absolute counting error (MAE) and normalized mean absolute error (NAE)

are used to evaluate the scene-level counting performance, comparing the scene-level predicted and ground-truth counts:

$$\text{MAE} = \frac{1}{N} \sum_{i=1}^N |\hat{c}_i - c_i|, \quad (11)$$

$$\text{NAE} = \frac{1}{N} \sum_{i=1}^N \frac{|\hat{c}_i - c_i|}{c_i}, \quad (12)$$

where c_i is the ground truth count and \hat{c}_i is the predicted count.

4.3 Experiment results

The experimental results are shown in Table 3 and the visualization results are found in the Figures 8, 9 and 10.

On **PETS2009**, the proposed 3D multi-view counting method can achieve better results than the two baseline multi-view counting methods (“Dmap weighted”, “Detection + ReID”) and the 3 versions of the end-to-end multi-view counting method proposed by Zhang and Chan (2019). The first two baseline methods cannot effectively fuse the multi-view information, which limits their performance. The proposed method achieves better performance than MVMS (Zhang and Chan 2019), which shows the advantage of the 3D projection and 3D fusion.

On **DukeMTMC**, our 3D multi-view counting method achieves slightly better performance than MVMS (Zhang and Chan 2019). The proposed method still achieves better performance than the two baseline methods. Due to low crowd count and lack of occlusions in the DukeMTMC, the performance gap is not very obvious. Looking at the 3D predictions in Fig. 9 (side view), our model can successfully predict people at different ground heights, which is consistent with the staircase and change in ground-level of the scene.

On **CityStreet**, our 3D multi-view counting method achieves the best results among the end-to-end multi-view counting methods (late fusion, naive early fusion, MVMS) and the two baseline methods. “Detection + ReID” performs poorly on CityStreet due to large crowd count and severe occlusions.

On **CVCS**, the backbone model with our 3D fusion achieves better performance than the original backbone of Zhang and Chan (2021). Since the 3D fusion is not proposed for cross-view cross-scene task, the performance is inferior to the CVCS model that contains extra modules for specifically handling cross-scene and cross-view data. Integrating the CVCS modules with the 3D fusion is interesting future work.

Method	MAE	NAE
Backbone	14.13	0.115
Backbone+3D fusion	13.30	0.123
CVCS	7.22	0.062

Table 5 The result comparison on the CVCS dataset. “Backbone” and “CVCS” are the models from Zhang and Chan (2021), where “Backbone” is the baseline model without any other extra modules to handle the cross-scene or cross-view data. “Backbone+3D fusion” is the method replacing 2D fusion in the “Backbone” model of Zhang and Chan (2021) with our 3D fusion.

4.4 Ablation study

In this section, we perform various ablation studies on the training loss, the ground-truth settings, height map estimation, and geometric attention.

4.4.1 Training loss.

We first compare training with different losses. The columns of Table 4 show the results of using 3D loss, 3D+2D loss or 3D+2D+PCM loss on the 3 datasets. Using single-view prediction branches and 2D supervision (3D+2D loss) can achieve better multi-view counting performance in comparison with only using 3D loss. Furthermore, using 3D+2D together with PCM loss can obtain better multi-view counting performance compared to using only 3D loss or 3D+2D loss on all 3 datasets with different ground-truth settings.

We next perform an ablation study on the weights of the loss terms on the PETS2009 and CityStreet datasets. The final loss contains 3D counting and 2D counting losses, height map estimation loss and projection consistency loss. The 2D counting loss is used to encourage extraction of useful counting features during training of the 3D counter. For simplicity, we use 0.01 as the 2D counting loss weights for all datasets. Since we use a pre-trained counter, then the 2D count loss is used to keep the features informative for 2D counting.

For the height map estimation loss, Table 7 shows the results using different values of weight σ . When σ is too small, the height estimation module is not well trained, and the model performance is limited. In contrast, when σ is too large, the 3D counting estimation is not well trained, so the performance drops. In the end, we select $\sigma = 5000$ for PETS2009 and $\sigma = 1000$ for CityStreet. For the projection consistency loss (PCM), we perform an ablation study on the weight γ in Table 8. When γ is too small, the model performance is limited because PCM loss has little influence. When γ is too large, the error caused by the projection (eg. calibration error) is introduced in the model training. We



Fig. 7 Examples of 3 multi-view datasets.

Dataset	PETS2009		DukeMTMC		CityStreet	
	3D+2D	3D+2D+PCM	3D+2D	3D+2D+PCM	3D+2D	3D+2D+PCM
without	3.20	3.15 ($\gamma = 100$)	1.03	1.01 ($\gamma = 0.1$)	7.58	7.54 ($\gamma = 10$)
with	3.15	3.20 ($\gamma = 100$)	0.94	0.92 ($\gamma = 0.1$)	7.15	7.12 ($\gamma = 10$)

Table 6 Ablation study: MAE for the proposed method with and without the geometric attention module. Two kinds of loss functions are used with/without the geometric attention: 3D+2D and 3D+2D+PCM losses. The parameter σ of the height map estimation loss l_{hmap} is 1000 for CityStreet, 5000 for PETS2009, and 10 for DukeMTMC.

σ	100	1000	5000	10000	20000
PETS2009	3.81	3.58	3.15	3.40	5.66
CityStreet	8.07	7.15	7.50	7.80	7.82

Table 7 Ablation study on the weight σ for the height map estimation loss on PETS2009 and CityStreet dataset.

γ	1	10	100	200	500
PETS2009	3.45	3.52	3.20	3.30	3.59
CityStreet	7.22	7.27	7.12	7.21	7.33

Table 8 Ablation study on weight γ for the height map estimation loss on PETS2009 and CityStreet dataset.

select $\gamma = 100$ for PETS2009 and $\gamma = 10$ for CityStreet.

4.4.2 Ground-truth setting.

The columns of Table 4 show the results of using different resolution of the 3D density map (n is the number of voxels in the z -dimension, and h is the voxel height in the 3D world). For PETS2009, the best performance is achieved by using 7 voxels and voxel height 40cm

with 3D+2D+PCM loss ($\gamma = 100$). For DukeMTMC, using voxel number 36 and voxel height 10cm with 3D+2D+PCM loss ($\gamma = 0.1$) gives the best result. As to CityStreet, the best result is obtained by using voxel number 28 and voxel height 10cm with 3D+2D+PCM loss ($\gamma = 10$). Compared to DukeMTMC and CityStreet, the best performance of PETS2009 is achieved at $h=40$ cm. The people occlusion in PETS2009 is more severe and many people’s lower bodies are totally occluded from all views (e.g., the people in the middle). Thus, increasing the height resolution does not provide additional information of the body, but may introduce more noise (other people’s features) along the z -dim, thus leading to worse performance.

4.4.3 Geometric attention.

We compare the 3D counting model’s performance with/without the module for attention along view ray in Table 6. In addition to the height map estimation loss l_{hmap} , two kinds of loss combinations are considered,

Method	PETS2009	CityStreet
No Mask + MSE	3.15	7.15
No Mask + CE	3.99	9.25
Mask + MSE	4.17	7.72
Mask + CE	3.56	8.27

Table 9 Ablation study on the loss for the height map estimation module (no PCM loss). “Mask” means remove the background in the height map estimation loss and “No Mask” means keep the background in the loss. “CE” denotes cross entropy loss.

3D+2D and 3D+2D+PCM losses. The best ground-truth settings are used for each dataset as indicated by the ablation study in Section 4.4.2. For the loss l_{hmap} , the weight $\sigma = 1000$ for CityStreet, $\sigma = 5000$ for PETS2009, and $\sigma = 10$ for DukeMTMC.

Results in Table 6 show that the performance can be improved with the geometric attention module. Especially on the DukeMTMC dataset, the performance gain of the model with geometric attention module is significantly improved (about 10%) compared to results without the module. The reason is the height change in DukeMTMC is larger than in other datasets and the geometric attention selects more suitable height levels for fusion, benefitting the multi-view fusion. On the CityStreet dataset, the performance with geometric attention is better than without using it, with a gain of about 6%. On the PETS2009 dataset, since the people height variance is smaller and most people are occluded in the scene, the effect of geometric attention is not as obvious, albeit it still achieves slightly better performance when without PCM loss.

4.4.4 Height map estimation loss.

We have also performed an ablation study on the form of the height map estimation loss, either MSE or Cross Entropy (CE) loss, and whether to use a mask to only compute the loss in the people’s bounding boxes (i.e., ignoring background pixels). The results in Table 9 show that the model performance with CE loss is not better than with MSE loss. Furthermore, keeping background pixels in the predicted geometric attention maps can achieve better performance because the background can provide context information for multi-view fusion (to associate the same people or distinguish different people) in the next stage.

4.4.5 Geometric attention vs. spatial attention.

We have performed ablation experiments to show the effect of the height map supervision and compared with a common spatial attention module (w/ or w/o supervision) in Table 10. The spatial attention mod-

Method	PETS2009	CityStreet
Geometric Attention (w/)	3.15	7.15
Geometric Attention (w/o)	4.59	7.59
Spatial Attention (w/)	4.03	9.93
Spatial Attention (w/o)	5.03	8.08

Table 10 Ablation study on the attention module (no PCM loss). “w/” and “w/o” indicate with supervision or without attention supervision, respectively.

ule estimates the 2D occupancy maps of the crowd and then projects them to the 3D world as attention. From Table 10, the performance of the proposed geometric attention module is better than the spatial attention module (regardless of with or without supervision). Furthermore, without the height map supervision, the performance of the geometric attention module drops, because the height map estimation needs extra information to distinguish the body parts of the people which projected to different height levels.

5 Conclusion and Discussion

In this paper, a DNN-based 3D multi-view counting method is proposed, which fuses camera-views to predict the 3D scene-level density map. 3D projection and fusion are used, which can handle the situation when people are not all located at the same height (e.g., people standing on a staircase), and provides a chance to solve the scale variation issue in the 3D space without a scale selection operation. The projection consistency measure between the 3D prediction and 2D density map ground-truth is studied and then utilized in the loss function to refine the 3D prediction further. Compared to other state-of-art multi-view counting methods, the proposed method achieves better or comparable counting performance as well as a more informative scene-level crowd representation.

In addition to counting humans, the proposed 3D multi-view counting method can also be applied to counting birds in the sky or the fish in the aquarium, where both the bird or the fish count can be obtained as well as their 3D location distributions – of course, this requires collecting more multi-view scenes. In addition to object counting, since the 3D Gaussian kernels are used as ground-truth, the 3D prediction provides a vivid visualization for the scenes, as well as the potentials for other applications like observing the scene in arbitrary view angles, which may contribute to better scene understanding, generation or visualization.

Acknowledgements This work was supported by grants from the Research Grants Council of the Hong Kong Special Administrative Region, China (CityU 11212518, CityU 11215820), and by a Strategic Research Grant from City University of Hong Kong (Project No. 7005665).

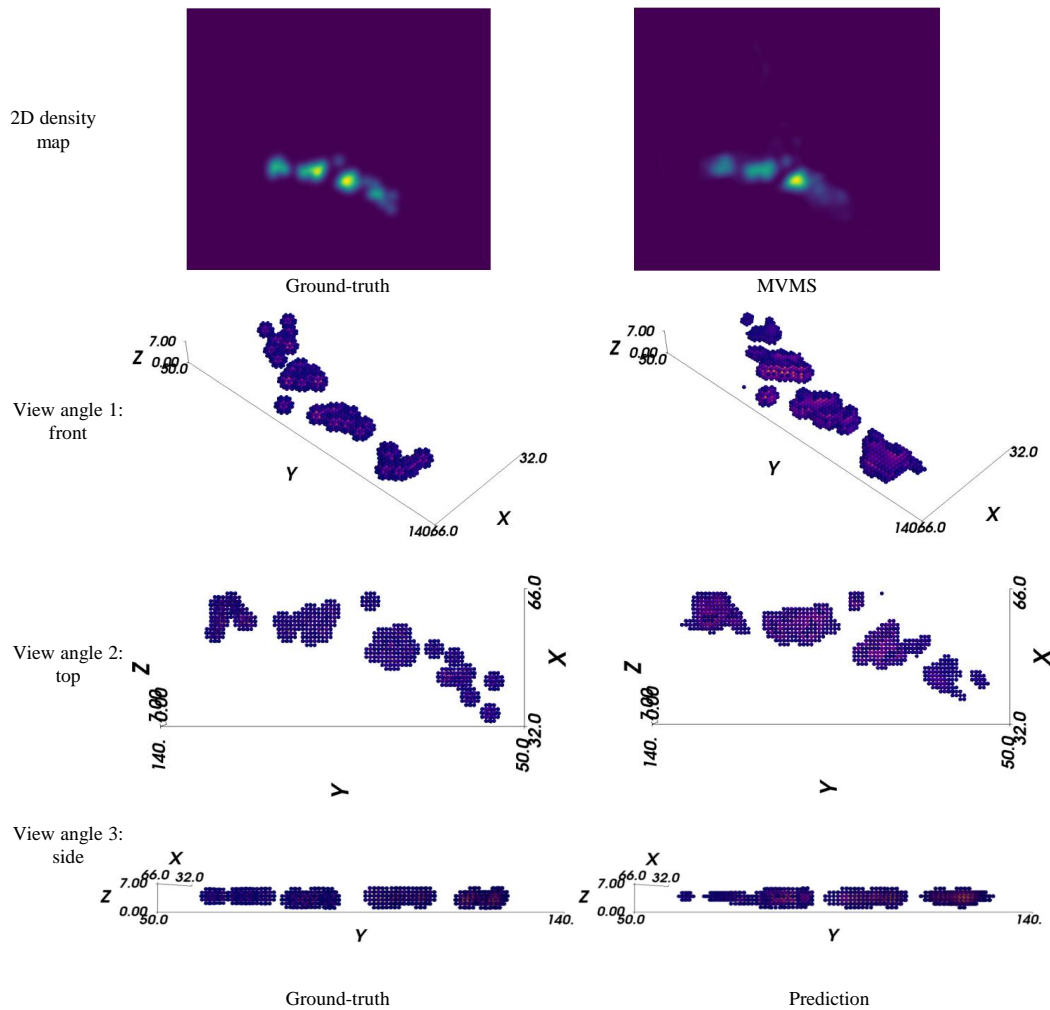


Fig. 8 Examples of the ground-truth and the predictions on PETS2009. The 3D density maps of PETS2009 are thresholded by $5e-3$, which are shown in 3 view angles: front, top and side. The 2D density map ground-truth and the prediction of the comparison method MVMS are also shown.

References

- Bai S, He Z, Qiao Y, Hu H, Wu W, Yan J (2020) Adaptive dilated network with self-correction supervision for counting. In: Proceedings of the IEEE/CVF Conference on Computer Vision and Pattern Recognition, pp 4594–4603 3
- Boominathan L, Kruthiventi SS, Babu RV (2016) Crowdnet: A deep convolutional network for dense crowd counting. In: ACM Multimedia Conference, ACM, pp 640–644 3
- Cao X, Wang Z, et al (2018) Scale aggregation network for accurate and efficient crowd counting. In: ECCV, pp 734–750 3
- Chan AB, Liang ZSJ, Vasconcelos N (2008) Privacy preserving crowd monitoring: Counting people without people models or tracking. In: CVPR, pp 1–7 1
- Chang AX, et al (2015) Shapenet: An information-rich 3d model repository. arXiv preprint arXiv:151203012 4
- Chen K, Chen LC, Gong S, Xiang T (2012) Feature mining for localised crowd counting. In: BMVC 1
- Choy CB, Xu D, Gwak J, Chen K, Savarese S (2016) 3d-r2n2: A unified approach for single and multi-view 3d object reconstruction. In: ECCV, Springer, pp 628–644 4
- Dittrich F, de Oliveira LE, Britto Jr AS, Koerich AL (2017) People counting in crowded and outdoor scenes using a hybrid multi-camera approach. arXiv preprint arXiv:170400326 3
- Ferryman J, Shahrokni A (2009) PETS2009: Dataset and challenge. In: IEEE International Workshop on Performance Evaluation of Tracking and Surveillance, pp 1–6 4, 9
- Ge W, Collins RT (2010) Crowd detection with a multiview sampler. In: ECCV, pp 324–337 2, 3
- Girdhar R, Fouhey DF, Rodriguez M, Gupta A (2016) Learning a predictable and generative vector representation for objects. In: ECCV, Springer, pp 484–499 5
- Huang PH, Matzen K, et al (2018) Deepmvms: Learning multi-view stereopsis. In: CVPR, pp 2821–2830 4
- Idrees H, et al (2018) Composition loss for counting, density map estimation and localization in dense crowds. In: ECCV, pp 532–546 1, 3
- Idrees H, Saleemi I, Seibert C, Shah M (2013) Multi-source multi-scale counting in extremely dense crowd images. In: CVPR, pp 2547–2554 1

- Iskakov K, Burkov E, Lempitsky V, Malkov Y (2019) Learnable triangulation of human pose. In: ICCV 2, 4
- Jaderberg M, Simonyan K, Zisserman A, Kavukcuoglu K (2015) Spatial transformer networks. In: Advances in Neural Information Processing Systems, pp 2017–2025 6
- Jiang X, et al (2019) Crowd counting and density estimation by trellis encoder-decoder networks. In: CVPR, pp 6133–6142 3
- Jiang X, Zhang L, Xu M, Zhang T, Lv P, Zhou B, Yang X, Pang Y (2020) Attention scaling for crowd counting. In: Proceedings of the IEEE/CVF Conference on Computer Vision and Pattern Recognition, pp 4706–4715 3
- Kang D, Chan A (2018) Crowd counting by adaptively fusing predictions from an image pyramid. In: BMVC 3
- Kang D, Dhar D, Chan A (2017) Incorporating side information by adaptive convolution. In: Advances in Neural Information Processing Systems, pp 3867–3877 3
- Kar A, Häne C, Malik J (2017) Learning a multi-view stereo machine. In: NIPS, pp 365–376 2, 4
- Li J, Huang L, Liu C (2012) People counting across multiple cameras for intelligent video surveillance. In: IEEE Ninth International Conference on Advanced Video and Signal-Based Surveillance (AVSS), IEEE, pp 178–183 2, 3
- Li Y, Zhang X, Chen D (2018) Csrnet: Dilated convolutional neural networks for understanding the highly congested scenes. In: CVPR, pp 1091–1100 3, 9
- Lian D, Li J, Zheng J, Luo W, Gao S (2019) Density map regression guided detection network for rgb-d crowd counting and localization. In: CVPR, pp 1821–1830 3
- Liao S, Hu Y, Zhu X, Li SZ (2015) Person re-identification by local maximal occurrence representation and metric learning. In: CVPR, pp 2197–2206 9
- Lim JJ, Pirsiavash H, Torralba A (2013) Parsing IKEA Objects: Fine Pose Estimation. In: ICCV 4
- Liu C, et al (2019) Recurrent attentive zooming for joint crowd counting and precise localization. In: CVPR, pp 1217–1226 3
- Liu J, Gao C, Meng D, Hauptmann AG (2018) Decidenet: Counting varying density crowds through attention guided detection and density estimation. In: CVPR, pp 5197–5206 3
- Liu W, Salzmann M, Fua P (2019) Context-aware crowd counting. In: CVPR, pp 5099–5108 3
- Liu X, Yang J, Ding W (2020) Adaptive mixture regression network with local counting map for crowd counting. arXiv preprint arXiv:200505776 3
- Ma H, Zeng C, Ling CX (2012) A reliable people counting system via multiple cameras. ACM Transactions on Intelligent Systems and Technology (TIST) 3(2):31 3
- Ma Z, Wei X, Hong X, Gong Y (2019) Bayesian loss for crowd count estimation with point supervision. In: Proceedings of the IEEE/CVF International Conference on Computer Vision, pp 6142–6151 3
- Maddalena L, Petrosino A, Russo F (2014) People counting by learning their appearance in a multi-view camera environment. Pattern Recognition Letters 36:125–134 3
- Onoro-Rubio D, López-Sastre RJ (2016) Towards perspective-free object counting with deep learning. In: ECCV, Springer, pp 615–629 3
- Ranjan V, Le H, Hoai M (2018) Iterative crowd counting. In: ECCV, pp 270–285 3
- Ren S, He K, Girshick R, Sun J (2015) Faster r-cnn: Towards real-time object detection with region proposal networks. In: Advances in neural information processing systems, pp 91–99 9
- Ristani E, Solera F, et al (2016) Performance measures and a data set for multi-target, multi-camera tracking. In: ECCV workshop on Benchmarking Multi-Target Tracking 9
- Ryan D, Denman S, Fookes C, Sridharan S (2014) Scene invariant multi camera crowd counting. Pattern Recognition Letters 44(8):98–112 2, 3
- Sam DB, Surya S, Babu RV (2017) Switching convolutional neural network for crowd counting. In: CVPR, pp 4031–4039 3
- Shen Z, Xu Y, Ni B, Wang M, Hu J, Yang X (2018) Crowd counting via adversarial cross-scale consistency pursuit. In: CVPR, pp 5245–5254 3
- Shi M, Yang Z, et al (2019) Revisiting perspective information for efficient crowd counting. In: CVPR, pp 7279–7288 3
- Sindagi VA, Patel VM (2017) Generating high-quality crowd density maps using contextual pyramid cnns. In: ICCV, pp 1879–1888 3
- Sindagi VA, Yasarla R, Babu DS, Babu RV, Patel VM (2020) Learning to count in the crowd from limited labeled data. arXiv preprint arXiv:200703195 3
- Sitzmann V, Thies J, Heide F, Nießner M, Wetzstein G, Zollhöfer M (2019) Deepvoxels: Learning persistent 3d feature embeddings. In: Proc. Computer Vision and Pattern Recognition (CVPR), IEEE 4
- Tang N, Lin YY, Weng MF, Liao HY (2014) Cross-camera knowledge transfer for multiview people counting. IEEE Transactions on Image Processing 24(1):80–93 2, 3
- Wang B, Liu H, Samaras D, Hoai M (2020) Distribution matching for crowd counting. arXiv preprint arXiv:200913077 3
- Wang Q, Gao J, et al (2019) Learning from synthetic data for crowd counting in the wild. In: CVPR, pp 8198–8207 3
- Xiong H, Lu H, Liu C, Liu L, Cao Z, Shen C (2019) From open set to closed set: Counting objects by spatial divide-and-conquer. In: Proceedings of the IEEE/CVF International Conference on Computer Vision (ICCV) 3
- Yan X, Yang J, et al (2016) Perspective transformer nets: Learning single-view 3d object reconstruction without 3d supervision. In: NIPS, pp 1696–1704 4
- Yang Y, Li G, Wu Z, Su L, Huang Q, Sebe N (2020) Reverse perspective network for perspective-aware object counting. In: Proceedings of the IEEE/CVF Conference on Computer Vision and Pattern Recognition, pp 4374–4383 3
- Zhang C, Li H, et al (2015) Cross-scene crowd counting via deep convolutional neural networks. In: CVPR, pp 833–841 1, 3
- Zhang Q, Chan AB (2019) Wide-area crowd counting via ground-plane density maps and multi-view fusion cnns. In: CVPR, pp 8297–8306 2, 4, 5, 6, 9, 10
- Zhang Q, Chan AB (2020) 3d crowd counting via multi-view fusion with 3d gaussian kernels. In: AAAI, pp 12837–12844 2, 5
- Zhang Q, Chan AB (2021) Cross-view cross-scene multi-view crowd counting. In: submitted to CVPR 2021 9, 10
- Zhang Y, et al (2016) Single-image crowd counting via multi-column convolutional neural network. In: CVPR, pp 589–597 1, 3

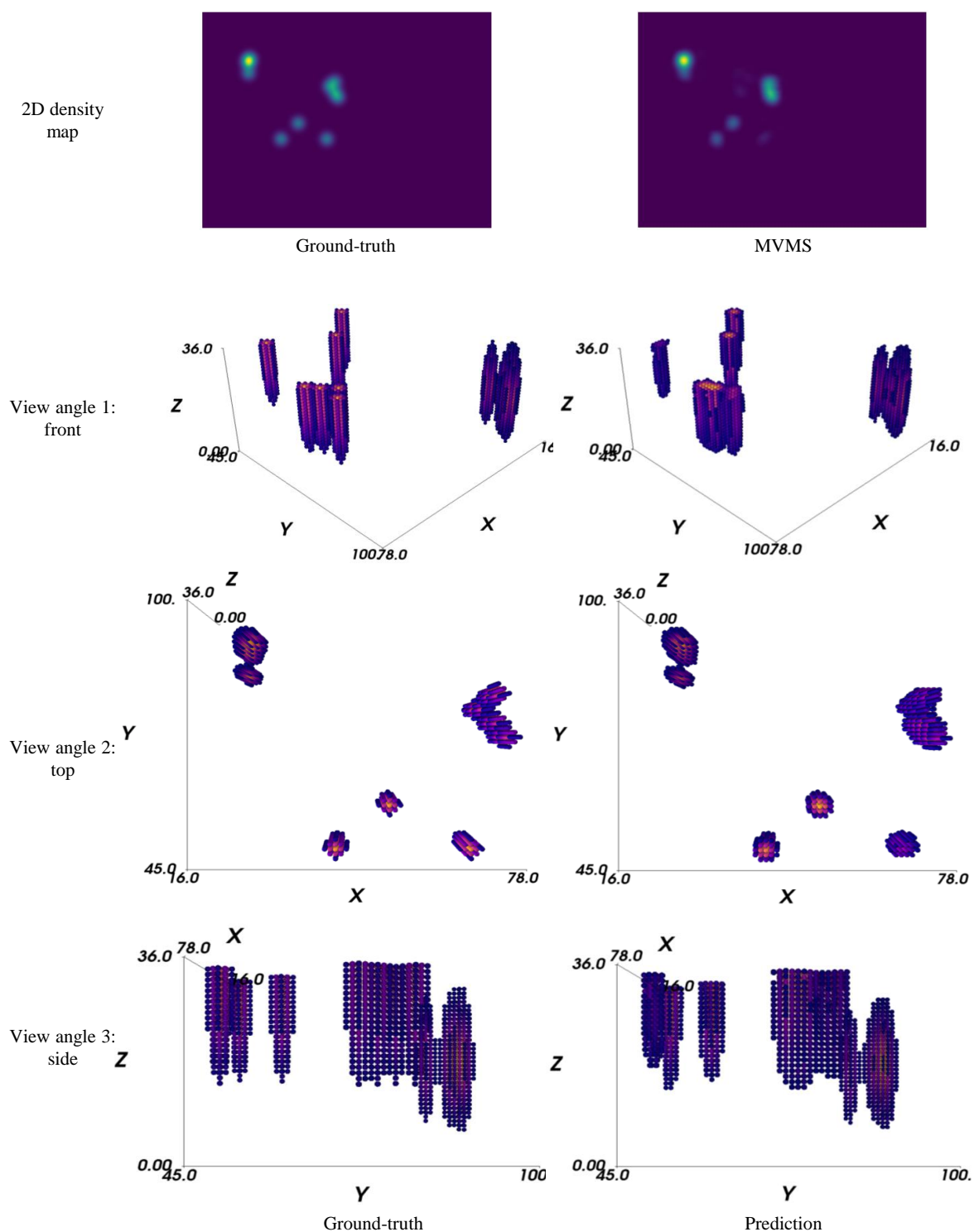


Fig. 9 Examples of the ground-truth and the predictions on DukeMTMC. The 3D density maps of DukeMTMC are thresholded by $1e-3$, which are shown in 3 view angles: front, top and side. The 2D density map ground-truth and the prediction of the comparison method MVMS are also provided. The third view angle (side) shows the variations in z-dimension of the people in the DukeMTMC dataset due to a staircase and raised ground-level.

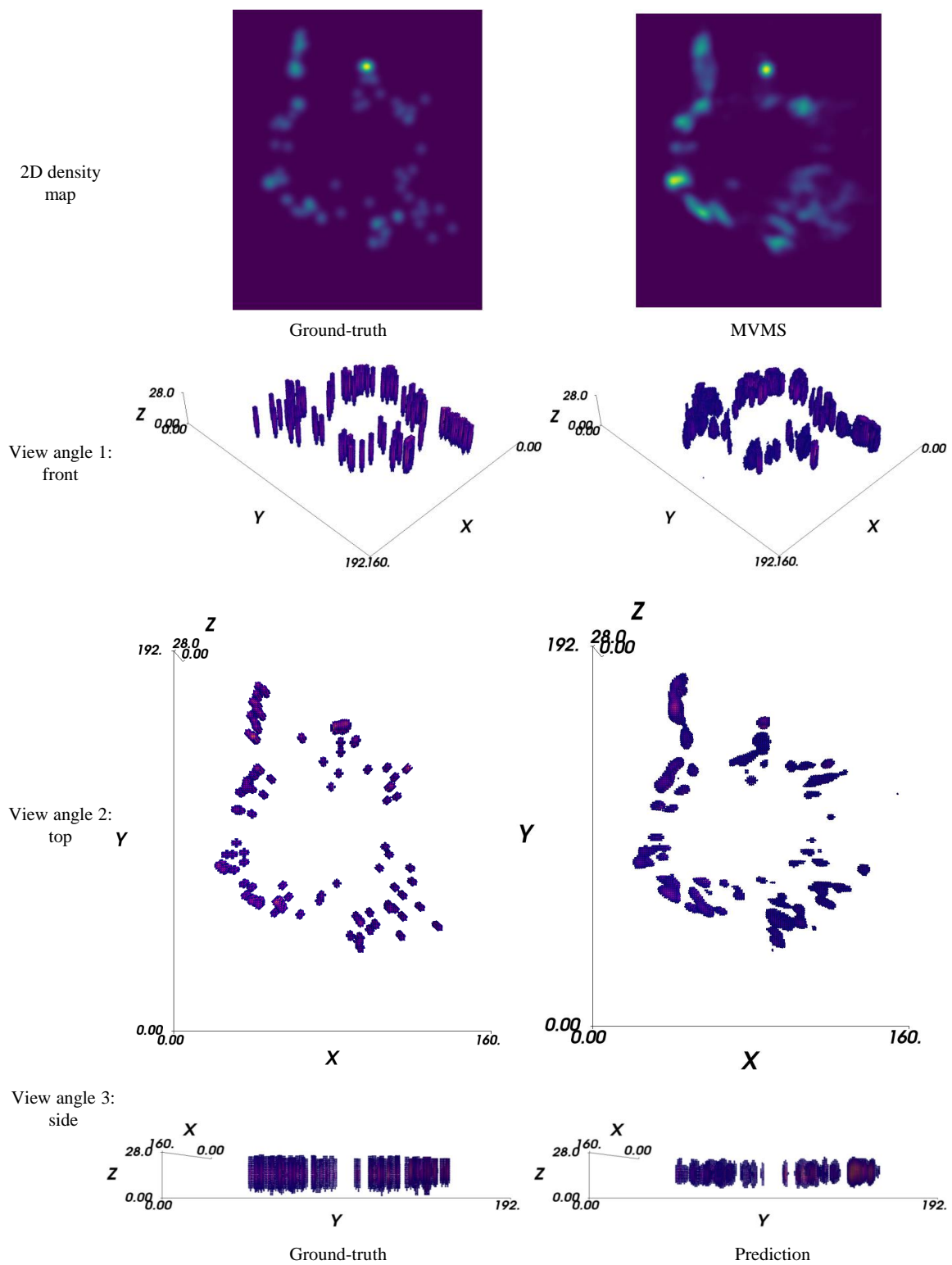


Fig. 10 Examples of the ground-truth and the predictions on CityStreet. The 3D density maps of CityStreet are thresholded by $2e-3$, which are shown in 3 view angles: front, top and side. The 2D density map ground-truth and the prediction of the comparison method MVMS are also shown.